# Identification and Analysis of Low-Frequency Cogging Torque Component in Permanent Magnet Machines

Devon R. McIntosh
Sonsight Inc. / NSWC
17609 Clinton Dr., Accokeek, MD 20607
devonrocky@gmail.com

**Abstract:** Cogging torque in permanent magnet motors and generators is characterized by a torque ripple that usually pulsates at a characteristically high angular frequency. This paper presents finite element (FE) analyses results that show a previously unaddressed low frequency modulation of cogging torque ripple. As cogging torque is minimized through successful application of optimization schemes, the relative proportion of the low-frequency component increases and becomes substantial. The current approach for analytically describing cogging torque does not allow for the modulation component. This paper extends this current approach so as to allow such a description. Modulation frequency and amplitude estimates are shown consistent with FE results.

**Keywords:** coggging torque, permanent magnet motors, torque ripple.

## 1. Introduction

Due largely to their high torque-to-current and torque-to-volume ratios, permanent magnet (PM) motors and generators are increasingly being used in a wide range of high performance applications such as industrial drives, robotics, computer peripherals, and automotive applications. However, most PM machines utilize a slotted iron structure with protruding teeth comprising the stator core that interacts with the PM poles on the rotor. This interaction generates a tendency for the rotor to align at preferential low energy detent positions relative to the stator slots. This is called cogging torque, and as the motor rotates, these torque fluctuations cause vibrations, noise and speed fluctuations. It can be a vital design consideration for machine startup and wherever accurate or constant speed motion control is required.

PM's with higher residual magnetic fields are increasingly being used to obtain motors with greater magnetic field intensities and therefore greater power densities. However, cogging torque is proportional to the square of the magnetic field intensity, and is therefore increasingly problematic. As a result, much time has been spent analyzing this problem, and developing techniques to minimize it. A number of techniques, supported by analytical and sometimes FE analysis and experimental results have been proposed and demonstrated [1] – [9]. These include optimizing the teeth width [1, 2, 3, 6], the pole width [2, 3, 4, 6, 7, 8], and the pole-to-teeth number ratio [2, 5, 6], and pairing teeth and poles of different widths [1, 2 and 4]. Also discussed are shaping the magnets [2, 7], notching the teeth [2, 4, 9], skewing the teeth or the poles [2, 4, 5, 7, 9], shifting the poles [4] and asymmetric motors [2]. Essentially all of these effects can be incorporated within a Fourier transformed air-gap field energy formulation described within several of the references and briefly reviewed below [1, 2, 3, 8]. However, as subsequently described, a low frequency modulation of the cogging torque ripple has been observed that is outside the scope of this prevailing formulation. This modulation, though relatively small compared with typical torque ripples, can constitute a significant portion of the minimized cogging torque amplitudes within motors optimized for reduced cogging torque.

The purpose of this paper is to characterize the low frequency modulation of the normal cogging torque ripple, and obtain an analytical formulation that explains it. As such a prior formulation of the normal high frequency ripple is introduced, then the observed modulation is presented. The extended formulation is then derived, and its results compared with those of FE analysis.

## 2. Standard Analysis of Cogging Torque

Cogging torque is generated by variations in the motor's magnetic field energy as the rotor turns. Since these energy variations are largely confined to the airgap and PM fields (i.e. the energy within the iron cores are typically considered negligible), the standard approach [1, 2, 3, 8] is to examine the energy in these fields $W_g$ due to the corresponding flux density distribution $B_g$:

$$W_g = \frac{1}{2\mu_0}\int B_g^2 dV \tag{1}$$

More explicitly (for a radial flux machine with PM permeability the same as air for example):

$$W_g(\alpha) = \frac{1}{4\mu_0} L_A (R_2^2 - R_1^2)\int_0^{2\pi} G^2(\theta) B_r^{'2}(\theta-\alpha) d\theta \tag{2}$$

where:
$\alpha$ = rotational angle of the rotor,
$\theta$ = angular position around the machine
$L_A$ = airgap length in axial direction,
For the external rotor machine, $R_2 = R_M$ and $R_1 = R_S$,
For the internal rotor machine, $R_2 = R_S$ and $R_1 = R_M$,
$R_M$ = PM radius, and $R_S$ = stator radius,
$G(\theta)$ = relative airgap permeance function (for instance, a simple functional form is to assume $G^2(\theta)$ is one constant value in the stator shoe areas and a smaller constant value in the stator slot areas, and both constant values are less than or equal to one [1, 2]),
$B_r^{'2}(\theta - \alpha)$ = modified PM remanence flux density (modified to include fringing field [3])

Cogging torque is given by :

$$T(\alpha) = -\frac{\partial W_g(\alpha)}{\partial \alpha} \tag{3}$$

The typical form of $G^2(\theta)$ (which we shall here define as $G_0^2$) can be expanded using Fourier series [1,2, 8] as:

$$G_0^2(\theta) = \sum_{n=0}^{\infty}\left[G_{anNs}\cos nN_S\theta + G_{bnNs}\sin nN_S\theta\right] \tag{4}$$

$B_r^{'2}(\theta - \alpha)$ can be likewise be expanded

$$B_r^{'2}(\theta-\alpha) = \sum_{n=0}^{\infty}\begin{bmatrix} B_{anNp}\cos nN_P(\theta-\alpha) \\ + B_{bnNp}\sin nN_P(\theta-\alpha)\end{bmatrix} \tag{5}$$

$N_S$ and $N_P$ are the number of slots and the number of PM's respectively. For symmetric machines the sin terms in (4) and (5) are zero. Utilizing (4) within (2) yields $W_{g0}(\alpha)$, i.e.:

$$W_{g0}(\alpha) = \frac{1}{4\mu_0} L_A (R_2^2 - R_1^2)\int_0^{2\pi} G_0^2(\theta) B_r^{'2}(\theta-\alpha) d\theta \tag{6}$$

Cogging torque can be determined by substituting the expansions (4) and (5) within (6) (trig angle subtraction identities are used to expand the trig functions in (5), and orthogonality relations are used in (6)), and then into (3) to obtain the cogging torque $T_0$ corresponding to the field energy $W_{g0.}$

$$W_{g0}(\alpha) = \frac{\pi L_A}{4\mu_0}(R_2^2 - R_1^2)\sum_{n=0}^{\infty} G_{anNL} B_{anNL}\cos nN_L\alpha \tag{7}$$

$$T_0(\alpha) = \frac{\pi L_A}{4\mu_0}(R_2^2 - R_1^2)\sum_{n=0}^{\infty} nN_L G_{anNL} B_{anNL}\sin nN_L\alpha \tag{8}$$

$N_L$ is the least common multiple of $N_S$ and $N_P$ (i.e. LCM{$N_S$, $N_P$}). It is now left to determine G and B for suitable permeance and B-field models [1, 2, 3, 8]. Expressions for the Fourier amplitudes provide an understanding of the means to minimize torque ripple, and leads to the above mentioned techniques. A more quantitative understanding is provided when used in conjunction with FE analysis.

The fundamental torque ripple frequency $N_L$ matches those obtained from experiments and FE analysis. For example, using the AC/DC module of COMSOL Multiphysics, a single-quadrant model of a 36 pole 28 slot machine (i.e. $N_P$=36, $N_S$=28, and therefore $N_L$= 252) shown in Fig. 1 produces the torque ripple shown in Fig. 2 via the electromagnetic stress tensor. The ~25.2 cycles occur over an angular displacement of

about 0.63 radians, yielding the requisite 252 cycles in $2\pi$ radians.

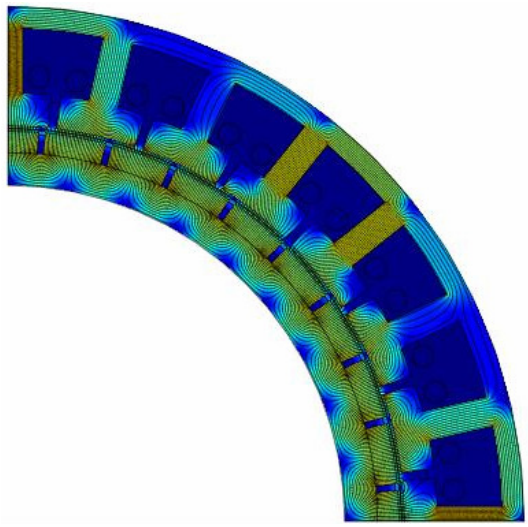

Fig. 1. Baseline version of PM machine quadrant (i.e. primary cell)

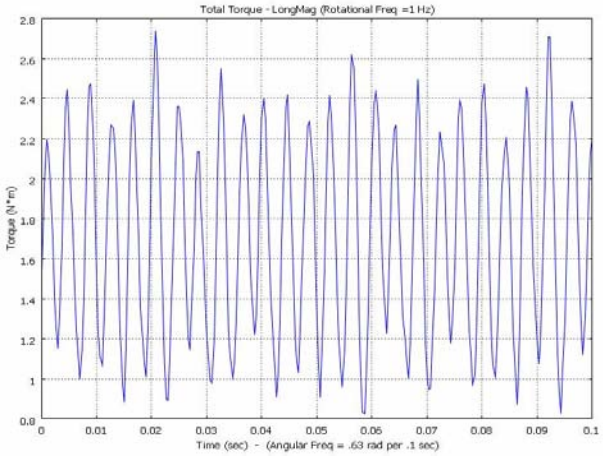


Fig. 2. Torque ripple over a period of.63 radians

## 3. Occurrence of Low Frequency Modulation

A closer inspection of Fig. 2 shows a low frequency modulation of the torque ripple. Some fluctuation of the ripple amplitude can be expected (as observed elsewhere [4]); however, this much is due to the machines ~300:1 ratio of machine torque to ripple amplitude. From the torque plot, the modulation does not seem to occur at a distinct frequency, but as shown from the energy plot in Fig. 3 (i.e. $W_g(\alpha)$), it is clear the modulation is of a single frequency. It seems the the modulation regularity is degraded when the rates of change of both components are combined in going from (2) to (3). Somewhat even more notable is that, for a version of the Fig. 1 machine with slightly convex shoes, Fig. 4 shows an energy plot with a more pronounced low frequency modulation. In this case, the modulation amplitude is greater than that of the normal high frequency ripple. However, there seems to be no published explanation for the modulation, and no analytical description of it. The approach used to obtain (7) and (8) contains no provision for any contribution to the cogging torque having an angular frequency less than $N_L$. For machines with minor cogging torque reduction this contribution may be negligible; however, for very low cogging machines, the low frequency component can add a substantial relative portion to overall cogging amplitude.

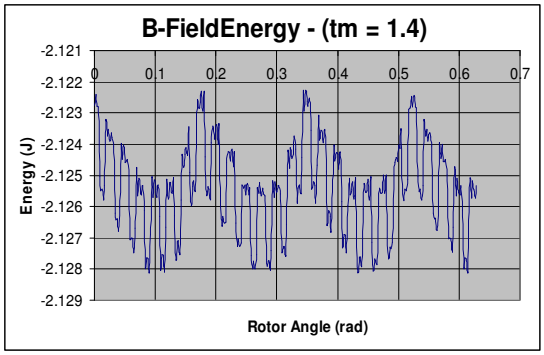


Fig. 3. $W_g(\alpha)$ for Fig. 1 model

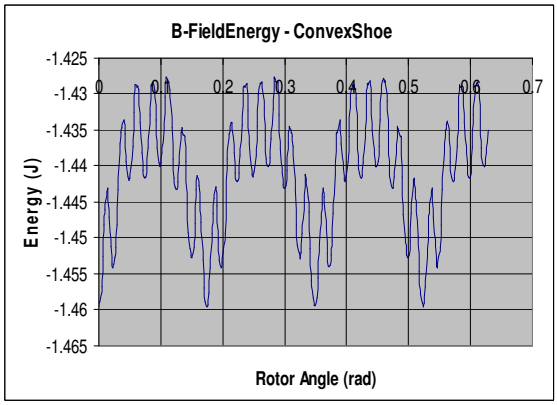


Fig. 4. $W_g(\alpha)$ for model similar to Fig. 1 but with slightly convex shoes

## 4. Extension of the Analytical Formulation

An extension of the above formulation is possible by starting with a more general form for $G^2(\theta)$ from a standard evaluation of the magnetic circuit along the flux path through the stator and rotor and across the airgap [10]. Such an expression for the gap flux $B_g$ can be written as:

$$B_g = \frac{B_r}{1+\frac{P_m}{P_g}+4\frac{P_{ml}}{P_g}} \tag{9}$$

where,

$P_m$ = PM permeance
$P_{ml}$ = magnet leakage permeance
$P_g$ = airgap permeance

$P_{ml}$ is associated with flux that leaks between adjacent magnets without going through the stator, and is modulated by the presence of the stator slots across the airgap. Only a fraction of the leakage flux $\Delta P_{ml}$ will vary with position relative to the slots, and together with a steady baseline value $P_{ml0}$ comprise $P_{ml}$ (i.e. $P_{ml}=P_{ml0}+\Delta P_{ml}$). (9) can be rewritten as:

$$B_g = B_r\left(1+\frac{P_m+4P_{ml0}}{P_g}\right)^{-1}\left(1+\frac{4\frac{\Delta P_{ml}}{P_g}}{1+\frac{P_m+4P_{ml0}}{P_g}}\right)^{-1} \tag{10}$$

Via $P_g$, the expression associated with the first set of parenthesis has a periodicity that is determined by that of the stator slots only. As such it corresponds to $G_0(\theta)$ used in the equations above and essentially to the permeance function used in the references [1, 2]; i.e:

$$G_0 = \left(1+\frac{P_m+4P_{ml0}}{P_g}\right)^{-1} \tag{11}$$

For θ within a shoe area, $P_g$, the denominator in (11), is much larger than the numerator (which is a constant value), and therefore $G_0(\theta)$ is close to unity. And for θ within a slot area, $P_g$ is much smaller than the numerator, and therefore $G_0(\theta)$ is close to zero. With (11), (10) can be rewritten as:

$$B_g = B_r G_0\left(1+4\frac{\Delta P_{ml}}{P_g}G_0\right)^{-1} \tag{12}$$

and,

$$B_g^2 \approx B_r^2 G_0^2\left(1-8\frac{\Delta P_{ml}}{P_g}G_0\right) \tag{13}$$

The magnet leakage flux that can be seen between adjacent magnets in Fig. 1 varies over the nine magnets within the modeled quadrant. The quadrant constitutes the primary cell for this machine, so the leakage flux pattern must repeat with a within the next quadrant. Also, since it is the presence of the stator that generates the leakage flux variation, the leakage flux is a periodic function of θ with a fundamental period that is one quadrant long. (13) can be rewritten as:

$$B_g^2(\theta,\alpha) = B_r^2(\theta-\alpha)G_0^2(\theta) - B_r^2(\theta-\alpha)G_1^2(\theta) \tag{14}$$

where,

$$G_1^2(\theta) = \frac{8\Delta P_{ml}(\theta)}{P_g}G_0^3(\theta) \tag{15}$$

Since the period of $\Delta P_{ml}$ (which must be the same as that of the leakage flux) must be an integral multiple of the period of $G_0^3$, the periodicity of $G_1^2$ is determined by that of $\Delta P_{ml}$ (i.e. the longest period). Substituting (14) into (1) yields:

$$W_g(\alpha) = W_{g0}(\alpha) - \left[\frac{1}{4\mu_0}L_A(R_2^2-R_1^2) \cdot \int_0^{2\pi} G_1^2(\theta)B_r'^2(\theta-\alpha)d\theta\right] \tag{16}$$

*or*,

$$W_g(\alpha) = W_{g0}(\alpha) - W_{g1}(\alpha)$$

Similar to (4), we expand $G_1^2$.

$$G_1^2(\theta) = \sum_{n=0}^{\infty}\left[G'_{anNc}\cos nN_c\theta + G'_{bnNc}\sin nN_c\theta\right] \tag{17}$$

where,

$N_C$ = GCF{$N_P$, $N_S$} = number of primary cells (in this case 4)

GCF = Greatest Common Factor

Similar to (7), substitution into (16) yields:

$$W_{g1}(\alpha) = \frac{\pi L_A}{4\mu_0}(R_2^2 - R_1^2)\sum_{n=0}^{\infty} G'_{anNP} B_{anNP} \cos nN_P\alpha \tag{18}$$

By definition, $N_P = LCM\{N_C, N_P\}$. This periodicity can be verified with inspection of Fig. (3) and Fig. (4) in which $N_C = 4$, $N_P = 36$. By definition, $N_P \leq N_L$, and therefore $W_{g0}(\alpha)$ must yield the high frequency ripples while $W_{g1}(\alpha)$ gives the low frequency modulation. As stated above, the fundamental frequency of the high frequency ripple is $N_L = 252$, while according to (18), that of the modulation is $N_P = 36$. The ripple frequency should therefore be seven times more than that of the modulation. This is borne out by the figures.

For comparison with Fig. 2, substitution of (16) with (18) into (3) gives the total torque:

$$T(\alpha) = T_0(\alpha) + T_1(\alpha)$$

where,

$$T_1(\alpha) = -\frac{\pi L_A}{4\mu_0}(R_2^2 - R_1^2)\sum_{n=0}^{\infty} nN_P G'_{anNP} B_{anNP} \sin nN_P\alpha \tag{19}$$

It is now left to check the relative amplitudes of the ripple and modulation components, which will be done only roughly. Subject to subsequent verification, the amplitude of $W_{g1}(\alpha)$ relative to $W_{g0}(\alpha)$ is assumed correlated with that of $G_1$ relative to $G_0$ (i.e. an appeal to (16)), which is in turn given by (15). Using the approximation that $G_0$ assumes values of either one or zero [1, 2],

$$W_{g1}/W_{g0} \approx G_1/G_0 \approx 8\Delta P_{ml}/P_g \tag{20}$$

Furthermore, by approximating a substantial linearity in the amplitude of $\Delta P_{ml}$ with respect to $P_{ml}$, (20) can be used to write,

$$\frac{W_{g1}}{W_{g0}} \propto \frac{P_{ml}}{P_g} \tag{21}$$

A simple form of this ratio obtained from a semicircular arc approximation of the fringing field [10] is:

$$\frac{P_{ml}}{P_g} = \frac{g}{\pi\tau_m}\ln\left[1 + \pi\frac{g}{\tau_p - \tau_m}\right] \tag{22}$$

$\tau_m$ is the magnet length, $\tau_p$ is the pole pitch (i.e. distance between adjacent magnet centers), and g is the airgap thickness.

Table 1 summarizes values obtained for several versions of the Fig. 1 generator model having different g and $\tau_m$ values, and compares the RHS ratio in (21) calculated via (22) with the LHS ratio in (21) obtained directly from FE analysis. This comparison is also provided graphically in Fig. 5. The last model was not included in the graph because it introduces an additional degree of freedom (i.e. shoe shape) that is not accounted for in (22), and which does not fit the simple linear relationship implied by (21).

Table 1

| Model | g (mm) | $\tau_p$ (mm) | $\tau_m$ (mm) | $P_{ml}/P_g$ | $W_{g1}/W_{g0}$ |
|---|---|---|---|---|---|
| Baseline | 3.18 | 39.90 | 25.40 | 0.02 | 0.47 |
| Long Mag | 3.18 | 39.90 | 35.91 | 0.04 | 0.44 |
| Long/Thin Mag | 6.99 | 39.90 | 35.91 | 0.12 | 1.75 |
| Thin Mag | 9.53 | 39.90 | 25.40 | 0.13 | 2.50 |
| Slightly Convex Shoe | 3.18 | 39.90 | 25.40 | 0.02 | 2.80 |

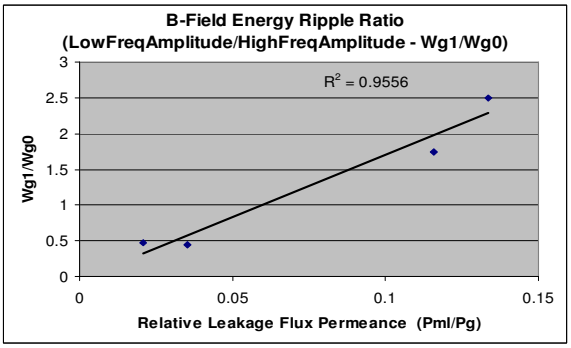


Fig. 5. Correlation of approximated amplitude ratios: Analytical vs. FE analysis

While not strictly proportional, Fig. 5 shows a strong correlation between the LHS and RHS

of (21), which strongly suggests that, in addition to the modulation frequency, the cogging torque and B-field energy modulation amplitudes derived from the extended analytical formulation are also correct. It provides a tool that can be used in conjunction with FE analysis to decrease both the low and high frequency cogging torque components. Fig. 5 shows that decreasing the leakage flux decreases the low frequency modulation, while the work summarized in Section 2 shows how to decrease the high frequency component. One deficiency of the model is the lack of an expression for $\Delta P_{ml}$. The assumed correlation with $P_{ml}$ in conjunction with (22) helps, but has limited applicability.

### 5. Use of COMSOL Multiphysics

The problem modeled in COMSOL is similar to a combination of two examples from the AC/DC Model Library: the *Generator in 2D*, and the *Generator with Mechanical Dynamics and Symmetry*; therefore, the governing E-M equation is the same quasi-static approximation used in those models. Only $1/4^{th}$ of the generator is modeled; therefore, the boundary conditions are the same as that of the latter model. However, a prescribed rotation exactly as described in the former model was used; therefore, unlike the latter model, no ODE for the mechanical dynamics was required. One interesting difference is that, there were many more structural features and dimensional variations than in the library models. This seemed to cause problems with the transient solver; therefore, because there was no need to model induced currents, the parametric solver was used instead with time as the parameter.

## 6. Conclusion

Low frequency cogging modulation in PM machines seems to have previously gone unaddressed. The current work accomplished the following:

1. Used FE analysis to identify and characterize low-frequency modulation of PM machine cogging torque,
2. Obtained an analytical formulation that describes and explains the modulation,
3. Demonstrated good agreement between the analytical formulation and the FE analysis for modulation frequency and amplitude,
4. Identified analytical relationships that provide a means of minimizing the low frequency cogging torque component.

## 7. References


1. S.M. Hwang, J.B. Eom, G.B.Hwang, W.B. Jeong, and Y.H. Jung, "Cogging Torque and Acoustic Noise Reduction in Permanent Magnet Motors by Teeth Pairing", *IEEE Trans. Mag*., **vol. 36**, No. 5, pp. 3144-3146, (2000).

2. S.M. Hwang, J.B. Eom, D.W. Lee, and B.S. Kang, "Various Design Techniques to Reduce Cogging Torque by Controlling Energy Variation in Permanent Magnet Motors", *IEEE Trans. Mag*., **vol. 37**, No. 4, pp. 2806-2809, (2001).

3. B. Ackerman, J.H.H. Janssen, R. Sottek, R.I. van Steen, "New technique for reducing cogging torque in a class of brushless DC motors", *IEEE Proc.*-B, **vol. 139**, No. 4, pp. 315-320, (1992).

4. N. Bianchi and S. Bolognani, "Design technique for reducing the cogging torque in sorface-mounted PM Motors", *IEEE Trans. Ind. Appl.,* **vol. 38**, No. 5, pp. 1259-1265, (2002).

5. D.C. Hanselman, "Effect of skew, pole count and slot count on brushless motor radial force, cogging torque and back EMF", *IEEE Proc.-Electr. Power Appl.*, **vol. 144**, No. 5, pp. 325-330, (1997).

6. C.C. Hwang, S.B. John, and S.S. Wu "Reduction of cogging torque in spindle motors for CD-ROM drive", *IEEE Trans. Mag*., **vol. 34**, No. 2, pp. 468-470, (1998).

7. A. Kumar, S. Marwaha, A. Marwaha, "Comparison of methods of minimization of cogging torque in wind generators using FE analysis", *J. Indian Inst. Sci.*, **vol. 86**, pp. 355-362, (2001).

8. Y. Yang, X. Wang, R. Zhang, T. Ding, R. Tang, "The optimization of pole arc coefficient to reduce coging torque in surface-mounted permanent magnet motors", *IEEE Trans. Mag*., **vol. 42**, No. 4, pp. 1135-1138, (2006).

2. S. Hwang, and D.K. Lieu, "Design techniques for reduction of reluctance torque in brushless in permanent magnet motors", *IEEE Trans. Mag*., **vol. 30**, No. 6, pp. 4287-4289, (1994).

10. D.C. Hanselman, *Brushless Permanent-Magnet Motor Design*, pp. 64-67. McGraw-Hill, New York (1994)